

# Liquid-phase reactions of aromatic organosulfates with OH radicals: Kinetics, mechanisms, and environmental effects

Yu Yang<sup>1</sup>, Caiqing Yan<sup>1</sup>, Ruyuan Yuan<sup>1</sup>, Ping Liu<sup>1</sup>, Hanyuan Zhang<sup>1</sup>, Haibiao Chen<sup>1</sup>, Yujiao Zhu<sup>1</sup>, Hengqing Shen<sup>1</sup>, Yan Wu<sup>2</sup>, Likun Xue<sup>1</sup> and Liubin Huang<sup>1\*</sup>

5 <sup>1</sup>Environment Research Institute, Shandong University, Qingdao, Shandong 266237, China

<sup>2</sup>School of Environmental Science and Engineering, Shandong University, Qingdao, Shandong 266237, China

*Correspondence to:* Liubin Huang (hliubin@sdu.edu.cn)

**Abstract.** Aromatic organosulfates (aromatic OSs) are widely detected in the atmosphere and exhibit high abundance in urban areas. However, the atmospheric fate and environmental impacts of aromatic OSs remain poorly understood. In this study, we investigated the liquid-phase reactions of three aromatic OSs (i.e., phenyl sulfate, p-tolyl sulfate, and 4-ethylphenyl sulfate) with OH radicals ( $\bullet\text{OH}$ ). The second-order reaction rate constants ( $k$ ) of aromatic OSs with  $\bullet\text{OH}$  were measured in the range of  $4.3\text{--}6.4 \times 10^9 \text{ M}^{-1} \text{ s}^{-1}$  at different pHs. It is found that  $k$  values are similar for the homologues of aromatic OSs, whereas they are slightly affected by the solution pH values. These three aromatic OSs oxidized by  $\bullet\text{OH}$  mainly yielded functionalized OSs, along with fragmented OSs and inorganic sulfate. The observation of inorganic sulfate formation, for the first time, indicates that aromatic OSs can also be converted into inorganic sulfate in analogous to aliphatic OSs. Furthermore, generated functionalized OSs can significantly enhance the light absorption capacity, particularly under acidic conditions. These findings provide new insights into the understanding of the fate of aromatic OSs in the atmosphere that they can rapidly undergo atmospheric transformation, affecting the atmospheric sulfur cycle and altering aerosol optical properties.

## 1 Introduction

20 Secondary organic aerosols (SOA) play a significant role in regional air quality, climate change, and public health (Peng et al., 2023; Shrivastava et al., 2017; Liu et al., 2022). Organosulfates (OSs), organic compounds characterized by a sulfate ester functional group ( $\text{R-O-SO}_3^-$ ), have been widely detected in SOA in various environments (from remote to highly polluted) (Kristensen et al., 2011; Zhang et al., 2012; Hansen et al., 2014; Hu et al., 2015; Wang et al., 2018; Ma et al., 2025), accounting for up to 30% of particulate organic mass (Surratt et al., 2008; Lukács et al., 2009; Tolocka and Turpin, 2012; Li et al., 2025). OSs can be produced from the reactions involving biogenic volatile organic compounds (VOCs) such as isoprene and monoterpenes, or anthropogenic VOCs such as diesel fuel vapor and aromatics (Hettiyadura et al., 2019; He et al., 2022; Wang et al., 2022; Thomas et al., 2025). In remote or clean areas, OSs were typically measured with the structure characterization of isoprene, monoterpenes, and their derivatives (Surratt et al., 2008; Zhang et al., 2012; Hettiyadura et al., 2017). For example, Thomas et al. (2025) reported that IEPOX-OS ( $\text{C}_5\text{H}_{12}\text{O}_7\text{S}$ ) is the dominant species of OSs in aerosols in Amazonian rainforest. In urban areas, in addition to isoprene and monoterpenes derived OSs, other OSs containing an aromatic ring were also

observed in collected aerosols (Kundu et al., 2013; Huang et al., 2018; Wang et al., 2021; He et al., 2022). He et al. (2022) identified four kinds of aromatic OSs (i.e., phenyl sulfate, methylphenyl sulfate, benzyl sulfate and phenethyl sulfate) with concentrations ranging from  $0.04 \pm 0.08$  to  $2.37 \pm 3.59$  ng m<sup>-3</sup> in PM<sub>2.5</sub> collected in Chengdu, China. Previous study observed that aromatic OSs can account for up to 63.5% of the total identified OSs in a megacity in China (Ma et al., 2014).

35 Extensive research has been conducted to elucidate the mechanisms of OSs in the atmosphere. The proposed formation mechanisms include: (a) the reactive uptake of epoxides on acidic sulfate aerosols. This pathway was established to be an important mechanism for the formation of isoprene-derived OSs (Surratt et al., 2010; Lin et al., 2013; Riva et al., 2019; Lei et al., 2022); (b) the multiphase reactions of unsaturated hydrocarbons with either sulfate radical ( $\bullet\text{SO}_4^-$ ) or sulfur dioxide (SO<sub>2</sub>). Previous studies revealed that the addition of  $\bullet\text{SO}_4^-$  on the C=C bond can result in the formation of OSs in aqueous aerosols  
40 (Nozière et al., 2010; Schindelka et al., 2013), and SO<sub>2</sub> can effectively react with unsaturated fatty acids to form OSs (Shang et al. 2016; Passananti et al. 2016); (c) heterogeneous reaction of organic peroxides with SO<sub>2</sub>. Recent laboratory studies have shown that SO<sub>2</sub> can also be oxidized by organic peroxides rapidly with the production of OSs other than sulfate (Wang et al., 2019; Yao et al., 2019, 2023); (d) substitution reaction of organic nitrates (ONs) by sulfate (Darer et al., 2011; Hu et al., 2011). Darer et al. (2011) and Hu et al. (2011) observed the formation of OSs during the processes of ON hydrolysis in the presence  
45 of H<sub>2</sub>SO<sub>4</sub>; (e) acid-catalyzed esterification of alcohols. While laboratory studies reported OS formation from sulfate esterification (Iinuma et al., 2007), subsequent kinetic study suggested that this reaction is too slow under typical tropospheric conditions (Minerath et al., 2008).

Compared to the formation of OSs, understanding of the fate of OSs is still limited. Hydrolysis has been identified as an atmospheric removal process for certain OSs, with rates depending on the acidity of the aerosol and the molecular structure  
50 (Darer et al., 2011; Hu et al., 2011; Mael et al., 2015). Tertiary OSs were found to hydrolyze effectively under acidic conditions, while primary and secondary OSs were relevantly stable. Additionally, OSs can also be further oxidized by OH radicals ( $\bullet\text{OH}$ ) after formation. Lai et al. (2024) investigated the kinetics of reactions of methyl sulfate and ethyl sulfate with  $\bullet\text{OH}$ , finding that the rate constant ( $k$ ) may be significantly affected by the carbon chain length. This finding was also verified in more kind of aliphatic OSs (i.e., methyl sulfate, ethyl sulfate, and propyl sulfate) (Gweme and Styler, 2024). Chen et al. (2020a) detected  
55 the products of 2-methyltetrol sulfate diastereomers (IEPOX-OS) oxidized by  $\bullet\text{OH}$  heterogeneously, observing varied fragmented and functionalized OSs after reactions, which their formation pathways were previously unknown in the atmosphere. During the oxidation of some OSs (e.g., methyl sulfate, ethyl sulfate, 2-methyltetrol sulfate, and  $\alpha$ -pinene derived OSs) by  $\bullet\text{OH}$ , it is interesting to find that OSs can also return to inorganic sulfate except for new OS formation (Kwong et al., 2018; Xu et al., 2020, 2024). In addition to laboratory studies, Tsona et al. (2025) employed quantum chemical calculation  
60 based on density functional theory to confirm the formation of inorganic sulfate from the gas-phase and aqueous-phase reactions of OSs with  $\bullet\text{OH}$ . It should be noted that the currently limited research about the fate of OSs has focused on the biogenic OSs or small alkyl OSs, little is known about the kinetic and mechanism for the conversion of aromatic OSs, which is another important kind of OSs, particularly in the urban aerosols. A very recent study investigated the aqueous-phase  $\bullet\text{OH}$  oxidation of phenyl sulfate other than aliphatic OSs (Gweme and Styler, 2024), observing that the  $k$  value of phenyl sulfate is

65 much faster than that of aliphatic OSs. After reactions, they observed the new OSs formed (hydroxyphenyl sulfate and dihydroxyphenyl sulfate), but without any evidence of inorganic sulfate production. However, whether aromatic OSs can be converted into inorganic sulfate or not remains unclear since they did not observe the presence of inorganic sulfate for aliphatic OSs as well. Therefore, to better characterize and understand the liquid-phase reactions of aromatic OSs and  $\bullet\text{OH}$ , further research is warranted.

70 In this study, we investigated the liquid-phase reactions of atmospherically relevant aromatic OSs (i.e., phenyl sulfate, p-tolyl sulfate, and 4-ethylphenyl sulfate) with  $\bullet\text{OH}$ . Our study aims to explore the influence of substituent structure on reaction kinetics and elucidate the mechanisms for the conversion pathways of aromatic OSs in the atmosphere. Moreover, given that the oxidation of aromatic organic compounds often induces significant alteration in the optical properties of the reaction system (Li et al., 2021; Arciva et al., 2024), the changes of optical properties were also examined.

## 75 **2 Materials and methods**

### **2.1 Batch reactor experiments**

Experiments of the liquid-phase  $\bullet\text{OH}$  oxidation of aromatic OSs were carried out in a 150 mL custom-built quartz reactor thermostated by a water jacket. OH radicals were generated through the aqueous photolysis of 10 mM  $\text{H}_2\text{O}_2$  (30%, Hu Shi) under irradiation from a 300 W Xenon arc lamp to simulate sunlight. Three commercial aromatic OSs (i.e., phenyl sulfate  
80 ( $\geq 98\%$ , Macklin), p-tolyl sulfate ( $\geq 98\%$ , Macklin), and 4-ethylphenyl sulfate ( $\geq 98\%$ , Sigma-Aldrich)) were used as the representatives of aromatic OSs. Their structures are shown in Fig. S1. The reaction solution containing each aromatic OS,  $\text{H}_2\text{O}_2$ , and dissolved  $\text{O}_2$  was introduced into the quartz reactor with a total volume of 100 mL, and was agitated by an electromagnetic stirrer. Subsequently, the reactor was sealed, and the lamp was then ignited to start the reaction. Given the varied pH values in aqueous environments in the atmosphere (from 1 to 9) (Herrmann et al., 2015; Pye et al., 2020), the solution  
85 was adjusted to pH 3 (using 36–38% HCl, Hu Shi) and pH 8 (using phosphate buffer ( $\text{Na}_2\text{HPO}_4$  and  $\text{NaH}_2\text{PO}_4$ )) to represent acidic and alkaline conditions, respectively. All experiments were performed at 298 K in at least duplicate. Details about the information of the experiments carried out in this study are summarized in Table S1.

Kinetic experiments were performed with 0.05 mM of each aromatic OS in the presence of reference compound (i.e., sodium benzoate (BA, 98%, Macklin)) in the reaction time of 2 hours. Two sets of control experiments were carried out. One involved  
90 irradiating a solution of each aromatic OS alone to investigate the effects of light only. Another set combined each aromatic OS and  $\text{H}_2\text{O}_2$  in the dark to preclude the interference of  $\text{H}_2\text{O}_2$ . Reaction progress was tracked by withdrawing 1 mL aliquots at 30-minute intervals for direct analysis via either ultrahigh-performance liquid chromatography (UPLC, Agilent 1260) or ion chromatography (IC, Dionex ICS-600), without any intermediate processes or dilution. Mechanism experiments were conducted the same as the kinetic experiments, except that BA was not added. After reactions, 0.5 mL of the sample was taken  
95 and was immediately stored at  $-20\text{ }^\circ\text{C}$  prior to product analysis using ultra-performance liquid chromatography equipped with quadrupole time-of-flight mass spectrometer (UPLC-Q-TOF-MS, Bruker Impact HD). Control experiments of each aromatic

OS and H<sub>2</sub>O<sub>2</sub> in the dark were also performed as the comparison in order to eliminate the possibility of detected products resulting from analytical artifacts. To enhance the detection of optical changes, we also conducted experiments at higher aromatic OS concentrations (0.5 or 1 mM) over an extended period of 8 hours. For these experiments, the sample was taken every 4 hours for immediate measurement of their absorbance spectra using UV–vis spectrophotometer (Duetta™, Horiba Scientific) and excitation–emission matrix (EEM) fluorescence spectra by a fluorescence spectrometer (Duetta™, Horiba Scientific). After reactions, the sample was also analyzed by ultrahigh-performance liquid chromatograph coupled with a photodiode array detector and an Orbitrap mass spectrometer (UPLC-PAD-MS, Thermo Fisher Scientific) to investigate how optical changes were affected by the formation of chromophores. 0.5 mL sample was diluted by 0.5 mL H<sub>2</sub>O and 0.25 mL acetonitrile, and then the resulting solution was stored at –20 °C before analysis.

## 2.2 Kinetic measurements

The second-order rate constant of each aromatic OS with •OH was measured by the competition kinetic method using 0.05 mM sodium benzoate as the reference compound (Smith et al., 2015). It is noted that one of important principles of this method is that aromatic OS and the reference compound are consumed only by •OH oxidation in the aqueous phase. Control experiments of the direct photolysis of each aromatic OS without the addition of H<sub>2</sub>O<sub>2</sub> as well as the reactions of each aromatic OS, BA, and 10 mM H<sub>2</sub>O<sub>2</sub> without illumination were carried out to preclude the interference of other reactions. Figures. S2 and S3 show that the influences of either hydrolysis or photodegradation on the kinetic measurements of these three aromatic OSs are negligible, verifying that the decay of reactants resulting from •OH oxidation. Therefore, in this study, the second-order rate constant for aromatic OS ( $k_{OS}$ ) can be calculated using the equation E1 based on the following reactions (R1 and R2).

$$\ln\left(\frac{[OS]_0}{[OS]_t}\right) = \frac{k_{OS}}{k_{ref}} \ln\left(\frac{[ref]_0}{[ref]_t}\right) \quad (E1)$$



Where [OS] and [ref] are concentrations of aromatic OS and the reference compound (BA) (time =0 and t). The time dependence of aromatic OS consumption is shown in Fig. S4.  $k_{ref}$  is the rate constant of BA with •OH.  $k_{ref}$  values at pH 3 and 8 were reported as  $4.3 \pm 0.8 \times 10^9 \text{ M}^{-1} \text{ s}^{-1}$  and  $6.3 \pm 0.2 \times 10^9 \text{ M}^{-1} \text{ s}^{-1}$ , respectively (Buxton et al., 1988). Figure 1 displays the relative kinetic plots for aromatic OSs oxidized by •OH under acidic (pH 3) and basic (pH 8) conditions. These plots exhibit strong linearity ( $R^2 \geq 0.99$ ), with the slope of each linear fit corresponding to the  $k_{OS}/k_{ref}$ . According to the slope and value of  $k_{ref}$ , the  $k_{OS}$  can be calculated.

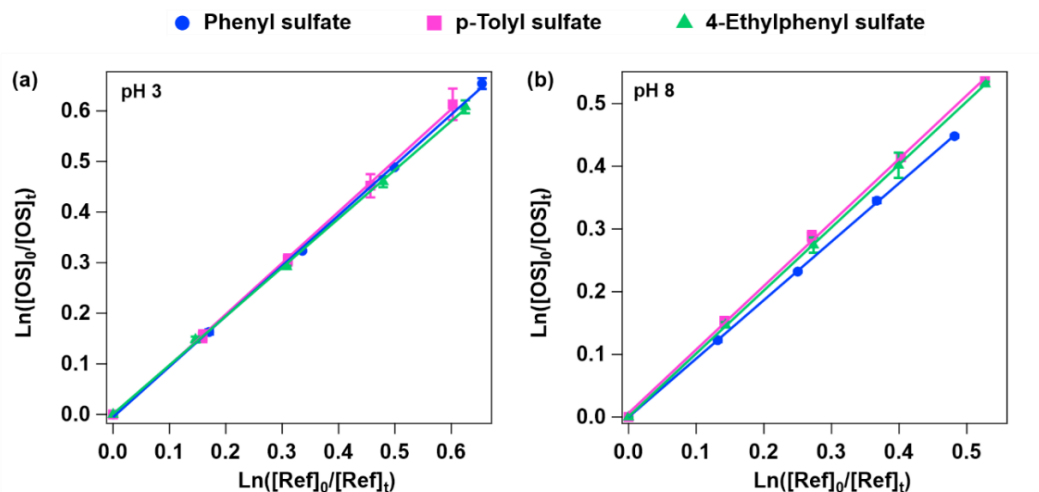


**Figure 1.** Loss of aromatic OSs and BA during the process of the liquid-phase  $\bullet\text{OH}$  oxidation at (a) pH 3 and (b) pH 8.

### 2.3 Reactant and product analysis

125 The concentrations of aromatic OSs and BA were detected using an ultrahigh-performance liquid chromatography (UPLC, Agilent 1260) coupled with a UV detector operating at 254 nm. Chromatographic separation was performed on a ZORBAX Eclipse Plus C18 column (4.6 mm  $\times$  250 mm, 5  $\mu\text{m}$ ) maintained at 40  $^{\circ}\text{C}$ . The mobile phase consists of acetonitrile and 0.1% formic acid aqueous solution (20:80, v/v) delivered at a flow rate of 0.8 mL  $\text{min}^{-1}$ , with an injection volume of 10  $\mu\text{L}$ . Quantification of aromatic OSs and BA was achieved by calibration curves (Fig. S5), based on their corresponding peak areas  
 130 in the chromatogram.

Inorganic sulfate was analyzed by IC with an analytical column (AS 11-HC, 4  $\times$  250 mm; IonPac) and a guard column (AG11-HC, 4 mm  $\times$  250 mm, IonPac). The eluent was 20 mM potassium hydroxide at a flow rate of 1 mL  $\text{min}^{-1}$ .

Reaction products were detected using a UPLC-Q-TOF-MS. Separation was achieved on a C18 column (4.6 mm  $\times$  250 mm, particle size = 5  $\mu\text{m}$ ; ZORBAX Eclipse Plus) at 40  $^{\circ}\text{C}$ , with a mobile phase of pure water and acetonitrile (40:60, v/v) at a flow  
 135 rate of 1 mL  $\text{min}^{-1}$ . The mass spectrometer was equipped with an electrospray ionization (ESI) source operated in the negative (-) ionization mode. The instrumental conditions for the (-) ESI-MS analysis were as follows: capillary voltage, 4000 V; gas temperature, 200  $^{\circ}\text{C}$ ; dry gas flow rate, 5 L  $\text{min}^{-1}$ ; and nebulizer pressure, 0.4 bar. Data were collected over the mass range of 50–500 Da. We also conducted complementary chromophore product analyses using a UPLC-PAD-MS. Separation was carried out a C18 column (4.6 mm  $\times$  250 mm, particle size = 5  $\mu\text{m}$ ; ZORBAX Eclipse Plus) at 40  $^{\circ}\text{C}$ , with a binary mobile  
 140 phase consisting of acetonitrile and 0.1% formic acid (20:80, v/v) delivered at a flow rate of 0.8 mL  $\text{min}^{-1}$ . Mass spectrometric detection was conducted in negative ionization mode over a mass range of 50–500 Da, with the spray voltage set at -3.0 kV, the capillary temperature at 320  $^{\circ}\text{C}$ , the S-lens RF level at -50V, the sheath gas (nitrogen) pressure at  $2.76 \times 10^5$  Pa, and the auxiliary gas (nitrogen) flow rate at 3.33 L  $\text{min}^{-1}$ .

## 2.4 UV-vis absorption and fluorescent spectra

145 The light absorption spectra of samples during the processes of reactions were collected using a UV-vis spectrophotometer with a scanning interval of 1 nm in the range of 250–700 nm. A reference absorption spectrum of hydrochloric acid solution (pH 3) or phosphate buffer solution (pH 8) was recorded in the same cuvette before sample analysis for baseline correction. The excitation-emission matrix (EEM) fluorescence spectra were recorded by a fluorescence spectrometer. The excitation wavelength (Ex) and emission wavelength (Em) of EEM were both set to the range of 250–600 nm. The scanning intervals  
150 were set to 5 nm and 2 nm. hydrochloric acid solution (pH 3) or phosphate buffer solution (pH 8) was used as a blank to correct the data as well.

## 3 Results and discussion

### 3.1 Kinetics of liquid-phase reaction of aromatic OSs with •OH

The  $k_{OS}$  values of three aromatic OSs (i.e., phenyl sulfate, p-tolyl sulfate, and 4-ethylphenyl sulfate) are summarized in Table  
155 1 reacted with •OH. At pH 3, the  $k_{OS}$  value of phenyl sulfate was measured as  $4.3 \pm 0.1 \times 10^9 \text{ M}^{-1} \text{ s}^{-1}$ . This value is comparable to the literature result of phenyl sulfate at pH 2 using pimelic acid as the reference compound ( $5.34 \pm 0.06 \times 10^9 \text{ M}^{-1} \text{ s}^{-1}$ ) (Gweme and Styler, 2024). The slight difference may be attributed to the reference compound selection and the experimental conditions. Values of  $k_{OS}$  for the other two aromatic OSs were similar to that of phenyl sulfate. The similar  $k_{OS}$  value among  
160 these three aromatic OSs suggests that the substituent carbon chain length on the aromatic ring has a negligible effect on the reaction kinetics. This observation is quite different from that for alkyl OSs, which shows that  $k_{OS}$  is strongly dependent on the carbon number of OS molecule contained (Armstrong et al., 2022; Yan et al., 2023; Lai et al., 2024; Gweme and Styler, 2024). Lai et al. (2024) reported that  $k_{OS}$  of ethyl sulfate ( $3.8 \pm 0.1 \times 10^8 \text{ M}^{-1} \text{ s}^{-1}$ ) was approximately five times higher than that of methyl sulfate ( $7.5 \pm 0.1 \times 10^7 \text{ M}^{-1} \text{ s}^{-1}$ ). Gweme and Styler (2024) also found that  $k_{OS}$  value increased with increasing carbon  
165 chain length for methyl sulfate ( $1.03 \pm 0.21 \times 10^8 \text{ M}^{-1} \text{ s}^{-1}$ ), ethyl sulfate ( $4.07 \pm 0.17 \times 10^8 \text{ M}^{-1} \text{ s}^{-1}$ ), and propyl sulfate ( $1.22 \pm 0.03 \times 10^9 \text{ M}^{-1} \text{ s}^{-1}$ ). This distinct behaviour may be ascribed to the different mechanisms for aromatic OSs and alkyl OSs oxidized by •OH. For aromatic OSs, the OH radical predominantly attacks the aromatic ring with multiple addition sites (Bloss et al., 2005; Garmash et al. 2020). While alkyl OSs react primarily through hydrogen abstraction, the increasing carbon chain length can enhance reactivity through the inductive effect of  $-\text{CH}_x$  groups, the increasing electron density at the hydrogen abstraction site, and the stabilization of resulting alkyl radicals (Monod and Doussin, 2008; Dorfman and Adams, 1973). As  
170 such, aromatic OSs has higher reactivity compared to alkyl OSs. The negligible effect of carbon number on the reactivity of aromatic compounds was also observed in other structure of homologue of aromatics. For example, Schuler and Albarran. (2002) reported a similar rate constant for the reactions of toluene ( $8.1 \times 10^9 \text{ M}^{-1} \text{ s}^{-1}$ ) and benzene ( $7.8 \times 10^9 \text{ M}^{-1} \text{ s}^{-1}$ ) with OH radicals. It is noted that the  $k_{OS}$  values are lower than those of their parent aromatic hydrocarbons. This reduction in reactivity

may be attributed to the electron-withdrawing effect of the  $-\text{OSO}_3^-$  groups, which can reduce the reactivity of the aromatic ring toward  $\bullet\text{OH}$  (Lai et al., 2024).

**Table 1. The second-order rate constant ( $k$ ) of aromatic OSs reacting with  $\bullet\text{OH}$  in the liquid phase at different pHs.**

Species	$k$ ( $10^9 \text{ M}^{-1} \text{ s}^{-1}$ )	
	pH = 3	pH = 8
Phenyl sulfate	$4.3 \pm 0.1$	$5.9 \pm 0.1$
p-Tolyl sulfate	$4.4 \pm 0.1$	$6.4 \pm 0.2$
4-Ethylphenyl sulfate	$4.5 \pm 0.1$	$6.3 \pm 0.1$
Benzoic acid <sup>a</sup>	$4.3 \pm 0.8$	$6.3 \pm 0.2$

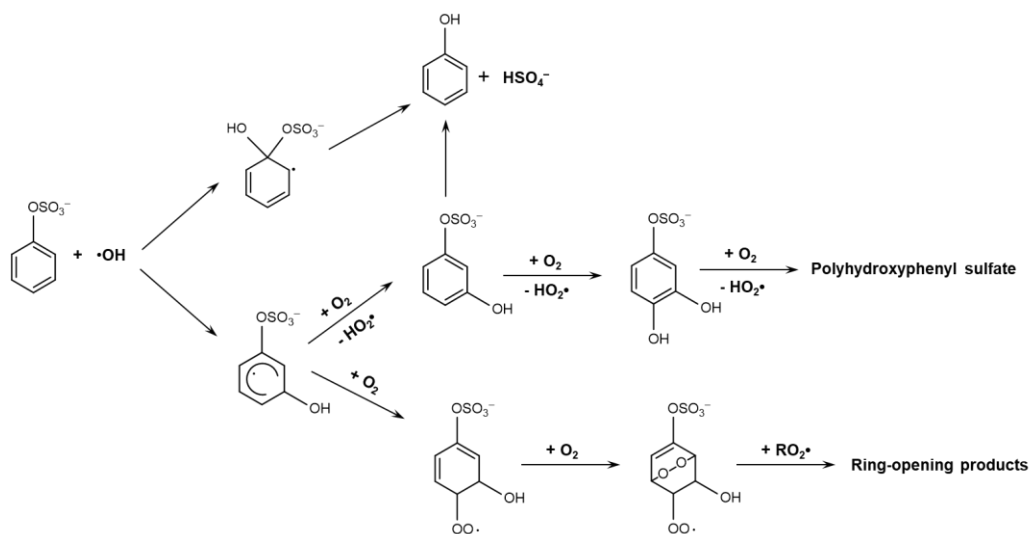
<sup>a</sup> Rate constants for benzoic acid are obtained from Buxton et al. (1988).

Table 1 shows that the carbon chain length has an insignificant effect on the  $k_{OS}$  values of aromatic OSs at pH 8 as well.  $k_{OS}$  values of phenyl sulfate, p-tolyl sulfate, and 4-ethylphenyl sulfate were calculated as  $5.9 \pm 0.1 \times 10^9$ ,  $6.4 \pm 0.2 \times 10^9$ , and  $6.3 \pm 0.1 \times 10^9 \text{ M}^{-1} \text{ s}^{-1}$ . These values were higher than those measured at pH 3. It should be noted that different matrices (HCl vs phosphate buffer) were used to adjust the solution pH, and the ionic strength of the solution is different at different pHs. The ionic strengths of solution at pH 3 and pH 8 were estimated as  $1 \times 10^{-3} \text{ M}$  and  $6.9 \times 10^{-3} \text{ M}$ , respectively. Previous study reported that a substantial increase in ionic strength from ca. zero to 6.5 M only resulted in a tenfold decrease in  $k_{OS}$  value of phenyl sulfate (Gweme and Styler, 2024). Therefore, the relatively low ionic strength variation between pH conditions in this study may not account for the observed differences in the  $k_{OS}$  values of aromatic OSs. Gweme and Styler (2024) measured the  $k_{OS}$  of phenyl sulfate at pH 2 and pH 9, observing that it was pH independence. They attributed this pH independence to phenyl sulfate remaining fully deprotonated ( $\text{pK}_a = -2.2$ ) across the entire experimental pH range. However, previous studies demonstrated that even though methoxyphenol, benzene-diols, and highly substituted phenol mainly exist in their protonated form within the pH range of 2–6, their  $k$  values at pH 2 was generally lower than those at pH 5 or 6 (Arciva et al., 2022). On possible explanation is that the acidic condition could hinder  $\bullet\text{OH}$  attack on aromatic systems or reduce the lifetime of hydroxyl-cyclohexadienyl radical intermediates, slowing irreversible diol formation (Smith et al., 2015). Another possible explanation is the uncertainty of the  $k$  of the reaction of reference compound with  $\bullet\text{OH}$  (Arciva et al., 2022). Therefore, the difference and uncertainty of the rate constant of the reference compounds selected may also explain the discrepancy between that reported by Gweme and Styler (2024) and our study.

### 195 3.2 Product measurements and reaction mechanism

In this study, products generated from the liquid-phase reactions of three aromatic OSs with  $\bullet\text{OH}$  were characterized by mass spectrometry. The identified species were consistent across both under pH 3 and pH 8 conditions. The observation that product intensities were substantially higher under illumination conditions than in dark controls implies that these products arise from  $\bullet\text{OH}$  oxidation, not from analytical artifacts or hydrolysis (Fig. S6). Table S2 lists the identified products from the reaction of phenyl sulfate with  $\bullet\text{OH}$ . The predominant signals corresponded to hydroxyphenyl sulfate ( $\text{C}_6\text{H}_5\text{O}_5\text{S}^-$ ,  $m/z$  189) and

dihydroxyphenyl sulfate ( $C_6H_5O_6S^-$ ,  $m/z$  205), aligning with previous work (Gweme and Styler, 2024). Additionally, the multiple  $-OH$  group addition products (e.g.,  $C_6H_5O_7S^-$ ,  $C_6H_7O_8S^-$ , and  $C_6H_7O_9S^-$ , were also detected. As illustrated in Fig. 2,  $\bullet OH$ -initiated oxidation of phenyl sulfate follows a mechanism analogous to conventional aromatic compounds (e.g., benzene). The reaction initiates via the addition of  $\bullet OH$  to the aromatic ring, generating hydroxycyclohexadienyl radicals (OH-PS radicals) (Lay et al., 1966; Minakata et al., 2015). OH-PS radicals rapidly react with  $O_2$  to yield phenolic compounds that can undergo further multi-step  $\bullet OH$  additions to form these polyhydroxy products ( $C_6H_5O_nS^-$ ,  $n=5-8$ ). Alternatively, OH-PS radicals can also react with  $O_2$  to form peroxy radicals ( $RO_2\bullet$ ). The reversible cyclization of  $RO_2\bullet$  and the subsequent  $O_2$  addition generate bicyclic  $RO_2\bullet$ . Bicyclic  $RO_2\bullet$  can react with  $RO_2\bullet$  to produce ring-opening products as shown in Table S2 (Wang et al. 2013; Dong et al. 2021). Fragmented OS formation resulting from ring-opening pathways during  $\bullet OH$  oxidation of aromatic OSs has not reported previously. Notably, some of these ring-opening fragments (e.g.,  $C_2H_3O_5S^-$ ,  $C_5H_7O_8S^-$ ) have the same formula of OSs detected in the atmosphere, which their precursors were regarded as biogenic VOCs (Kuang et al., 2016; Cai et al., 2020; Wang et al., 2022). For example, previous studies inferred that  $m/z$  139 ( $C_2H_3O_5S^-$ ) is produced from isoprene and its derivatives related reactions (Cai et al., 2020; Wang et al., 2022). In this study, we found that this compound can also be formed through the oxidation of phenyl sulfate by  $\bullet OH$ , providing the additional pathway for its formation in the atmosphere.



**Figure 2. Scheme for the mechanism of phenyl sulfate reacting with  $\bullet OH$ .**

Previous studies revealed that some aliphatic OSs (e.g., methyl sulfate, ethyl sulfate, 2-methyltetrol sulfate, and  $\alpha$ -pinene-derived OS) can be converted into inorganic sulfate during  $\bullet OH$  oxidation (Kwong et al., 2018; Xu et al., 2022, 2024; Lai et al., 2025). The reaction is initiated through hydrogen abstraction from the alkyl group, forming an alkyl radical ( $R\bullet$ ) followed by rapidly reacting with  $O_2$  to form  $RO_2\bullet$ . The self- or cross-reactions of  $RO_2\bullet$  can further produce an alkoxy radical ( $RO\bullet$ ). Typically, the formation of inorganic sulfate is resulted from the production of  $\bullet SO_4^-$ , which is generated from the

decomposition of  $\alpha$ -OSO<sub>3</sub><sup>-</sup> alkoxy radical (defined as the containing of -OSO<sub>3</sub><sup>-</sup> group at the  $\alpha$ -position of RO•). Additionally, a recent study proposed an alternative mechanism for the formation of inorganic sulfate, proceeding via sulfite radicals ( $\bullet$ SO<sub>3</sub><sup>-</sup>) (Xu et al., 2024). In this pathway, a  $\beta$ -OSO<sub>3</sub><sup>-</sup> alkoxy radical [-C(O•)-C(OSO<sub>3</sub><sup>-</sup>)-] undergoes C-C bond cleavage, yielding an  $\alpha$ -OSO<sub>3</sub><sup>-</sup> alkyl radical, subsequently generating non-sulfate products and  $\bullet$ SO<sub>3</sub><sup>-</sup>. Upon the formation of  $\bullet$ SO<sub>4</sub><sup>-</sup> and  $\bullet$ SO<sub>3</sub><sup>-</sup>, inorganic sulfate can be formed through the further reactions of these radicals. In this study, the formation of inorganic sulfate during the reaction of phenyl sulfate with  $\bullet$ OH was also examined. Figure S7a shows that the SO<sub>4</sub><sup>2-</sup> peak in IC increased progressively with reaction time. The formation of inorganic sulfate was further supported by the evidence of the observed prominent HSO<sub>4</sub><sup>-</sup> peak at  $m/z$  97, which is assigned to HSO<sub>4</sub><sup>-</sup>, in the mass spectra (Fig. S6b), the intensity in the extracted ion chromatograms (EIC) was substantially higher than in dark controls (Fig. S8a), ruling out in-source fragmentation or hydrolysis as the source of HSO<sub>4</sub><sup>-</sup>. The results of IC and mass spectrometry suggest that in addition to new OSs, inorganic sulfate can be formed during the reaction. The mechanism of inorganic sulfate formation is elucidated to be produced from the elimination of the sulfate group from phenyl sulfate, as well as the *ipso*-addition followed by disproportionation reaction as shown in Fig. 2. Phenyl sulfate can undergo *ipso*-addition to form OH-PS radical, the *ipso*-OH-adduct should either rapidly eliminate HSO<sub>4</sub><sup>-</sup>, or undergo bimolecular reactions with other isomers of the OH-PS radical to yield phenol upon elimination of HSO<sub>4</sub><sup>-</sup> as well. However, compared to other OH addition pathways (*o*-add, *m*-add, and *p*-add), there is only very little room for the *ipso*-addition. It is noted that previous study has shown that benzoic acid can undergo decarboxylation reactions (Singla et al., 2004). Another possible pathway for HSO<sub>4</sub><sup>-</sup> production is proposed to occur via the elimination of the sulfate group from phenyl sulfate, as similar to the decarboxylation mechanism of benzoic acid.

Tables S3 and S4 summarize the identified products from the liquid-phase reactions of *p*-tolyl sulfate and 4-ethylphenyl sulfate with  $\bullet$ OH, respectively. The mechanisms of *p*-tolyl sulfate and 4-ethylphenyl sulfate oxidized by  $\bullet$ OH are similar to that of phenyl sulfate as mentioned above. Similar to phenyl sulfate, the addition of  $\bullet$ OH to the aromatic ring predominantly yields phenolic compounds, such as C<sub>7</sub>H<sub>5</sub>O<sub>5</sub>S<sup>-</sup>, C<sub>7</sub>H<sub>7</sub>O<sub>5</sub>S<sup>-</sup>, C<sub>8</sub>H<sub>9</sub>O<sub>5</sub>S<sup>-</sup>, and C<sub>8</sub>H<sub>9</sub>O<sub>6</sub>S<sup>-</sup>. Further oxidation initiated by hydrogen abstraction can also generate fragmented products, such as C<sub>3</sub>H<sub>5</sub>O<sub>6</sub>S<sup>-</sup> and C<sub>4</sub>H<sub>5</sub>O<sub>7</sub>S<sup>-</sup> (Tables S2 and S3). Moreover, the presence of alkyl substituents for *p*-tolyl sulfate and 4-ethylphenyl sulfate can enable additional hydrogen abstraction pathways (Forstner et al., 1997; Baltaretu et al., 2009; Liu et al., 2017), leading to the formation of aromatic aldehydes (e.g., C<sub>7</sub>H<sub>5</sub>O<sub>5</sub>S<sup>-</sup>, C<sub>8</sub>H<sub>7</sub>O<sub>5</sub>S<sup>-</sup>). In addition to new OSs formed, the formation of inorganic sulfate was also observed during the process of either *p*-tolyl sulfate or 4-ethylphenyl sulfate oxidized by  $\bullet$ OH. For *p*-tolyl sulfate, the gradual increase of the SO<sub>4</sub><sup>2-</sup> peak with reaction time in IC as well as the pronounced signal of  $m/z$  97 (HSO<sub>4</sub><sup>-</sup>) observed in mass spectra provide robust evidences for the formation of inorganic sulfate during the reaction (Figs. S7b and S8b). For 4-ethylphenyl sulfate, SO<sub>4</sub><sup>2-</sup> peak in IC was found to overlap with that of the compound itself (Fig. S7c). The inference that 4-ethylphenyl sulfate converts to inorganic sulfate is supported by comparing the intensity of HSO<sub>4</sub><sup>-</sup> ( $m/z$  97) peak of samples collected from illumination and dark conditions (Fig. S8c).

### 255 3.3 Optical property changes

Kinetic and mechanism results show that aromatic OSs can undergo rapid  $\bullet\text{OH}$  oxidation to form a series of functionalized and fragmented compounds. The changes of optical properties resulting from the formation of these compounds were also investigated. Figure S9 shows the time-dependent absorption spectra of aromatic OSs during  $\bullet\text{OH}$  oxidation at pH 3. As the reaction progressed, the consume of reactants accompanied with the increase in absorbance across 250–400 nm. To establish  
260 the relationship between light absorption and organic compounds, chromophores formed in the reaction were identified by correlating UV absorption bands with the retention time based on UPLC-PAD-MS analysis. For phenyl sulfate, Figure 3a displays that phenyl sulfate ( $m/z$  173) was the prominent chromophore with the retention time of 5.67–6.16 min at the beginning of the reaction, exhibiting a characteristic absorption peak at 262 nm (Fig. S9a). After the liquid-phase  $\bullet\text{OH}$  oxidation, five major chromophores were observed as shown in Fig. 3c. Chromophore #4 was assigned to the unreacted phenyl sulfate. Figure  
265 3c shows that Chromophore #1, #2, and #3 eluted at 3.47–3.72 min, 4.00–4.18 min, and 5.46–5.60 min, respectively. These newly formed chromophores exhibit red-shifted absorption peaks (Fig. 10a), likely due to the electron-donating effect of hydroxyl groups increasing aromatic ring electron density (Hems and Abbatt, 2018). The results of EIC suggest that these chromophores correspond to co-eluting mixtures containing  $\text{C}_6\text{H}_5\text{O}_5\text{S}^-$  isomers ( $m/z$  189), along with  $\text{C}_6\text{H}_5\text{O}_6\text{S}^-$  ( $m/z$  205),  $\text{C}_6\text{H}_5\text{O}_7\text{S}^-$  ( $m/z$  221) and  $\text{C}_6\text{H}_7\text{O}_8\text{S}^-$  ( $m/z$  239) (Fig. 3d). Among these compounds,  $\text{C}_6\text{H}_5\text{O}_6\text{S}^-$  exhibited the highest intensity.  
270 Chromophore #5, eluting at 14.98–15.67 min, remained unidentified. Its later elution time suggests a larger molecular structure and lower polarity (Fleming et al., 2020). Additionally, there may exist other chromophores unidentified since these five chromophores can not fully explain the total light adsorption as shown in Fig. 10a.

For p-tolyl sulfate, the increase in absorbance, contributing by the formation of chromophores, was also observed after OH oxidation. The primarily newly formed chromophore (Chromophore #1), eluting at 5.23–5.78 min, was identified as  $\text{C}_7\text{H}_5\text{O}_5\text{S}^-$   
275 ( $m/z$  201) based on the corresponding EIC (Figs. S11c and d). A blue-shift peak at 258 nm was observed upon the formation of  $\text{C}_7\text{H}_5\text{O}_5\text{S}^-$ , which is associated with the generation of a carbonyl (C=O) functional group (Fig. S10b). Other newly formed chromophores were characterized as Chromophore #2 and Chromophore #3. Chromophore #2 corresponded to a mixture of  $\text{C}_7\text{H}_7\text{O}_5\text{S}^-$  ( $m/z$  203),  $\text{C}_7\text{H}_7\text{O}_5\text{S}^-$  ( $m/z$  217), and  $\text{C}_7\text{H}_7\text{O}_6\text{S}^-$  ( $m/z$  219) with absorption band at 274 nm, and Chromophore #3 was assigned to  $\text{C}_7\text{H}_7\text{O}_5\text{S}^-$  ( $m/z$  203) with the absorption band at 266 nm (Figs. S10b and S11). Figures S10c and S12 show the  
280 characterization of chromophores formed from liquid-phase reaction of 4-ethylphenyl sulfate with OH radicals. After reactions, Chromophore #2 ( $\text{C}_8\text{H}_7\text{O}_5\text{S}^-$ ,  $m/z$  215) with a characteristic absorption peak at 254 nm was the dominant contributor to total light absorption. Four additional chromophores were also identified: Chromophore #1, a mixture of  $\text{C}_7\text{H}_7\text{O}_5\text{S}^-$  ( $m/z$  201),  $\text{C}_8\text{H}_9\text{O}_5\text{S}^-$  ( $m/z$  217),  $\text{C}_8\text{H}_7\text{O}_6\text{S}^-$  ( $m/z$  231), and  $\text{C}_8\text{H}_9\text{O}_6\text{S}^-$  ( $m/z$  233), with absorption peak at 258 nm; Chromophore #3, an isomer of  $\text{C}_8\text{H}_7\text{O}_6\text{S}^-$ , with absorption peak at 262 nm; Chromophore #4, an isomer of  $\text{C}_8\text{H}_9\text{O}_5\text{S}^-$  ( $m/z$  217), with absorption  
285 peak at 274 nm; and Chromophore #5, another isomer of  $\text{C}_8\text{H}_9\text{O}_5\text{S}^-$ , also with a characteristic absorption peak at 274 nm.

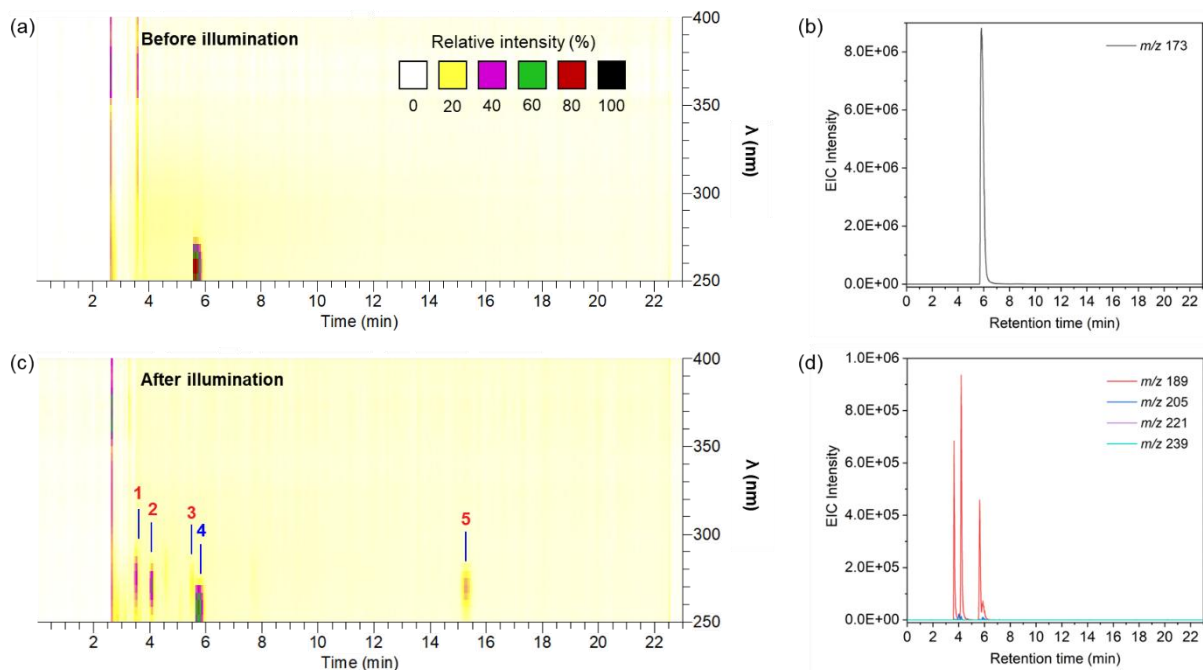


**Figure 3. UPLC-PAD-MS chromatograms of samples collected (a) before and (c) after the liquid-phase  $\bullet\text{OH}$  oxidation of phenyl sulfate at pH 3. The y-axis and color map represents the wavelength and corresponding UV-vis absorbance, respectively. Extracted ion chromatograms (EIC) of (b) phenyl sulfate and (d) the compositions of chromophores.**

290 Furthermore, fluorescence evolutions during liquid-phase  $\bullet\text{OH}$  oxidation of aromatic OSs were investigated as shown in Fig. 4. The initial maximum excitation/emission (Ex/Em) wavelengths of phenyl sulfate, p-tolyl sulfate, and 4-ethylphenyl sulfate at pH 3 were Ex/Em = 255/275 nm, 260/284 nm, and 260/284 nm, respectively. The different initial fluorescence intensity among these three aromatic OSs may be attributed to the substituent effect of the compound. Compared to phenyl sulfate, p-tolyl sulfate and 4-ethylphenyl sulfate contain additional methyl and ethyl groups, respectively. These electron-donating substituents extend the conjugation system, lowering the  $\pi \rightarrow \pi^*$  transition energy and resulting in both emission redshift and fluorescence enhancement (Cao et al., 2023). During the reaction, the fluorescence intensity initially decreased due to phenyl sulfate consumption, followed by a subsequent increase from fluorescent product formation. After 8 h of illumination, a redshifted fluorescence peak emerged at Ex/Em = 260/283 nm, implying the formation of products with expanded conjugated systems (e.g.,  $\text{C}_6\text{H}_5\text{O}_5\text{S}^-$ ,  $\text{C}_6\text{H}_5\text{O}_6\text{S}^-$  and  $\text{C}_6\text{H}_5\text{O}_7\text{S}^-$ ) (Tang et al., 2020). The fluorescence intensity of p-tolyl sulfate and 4-ethylphenyl sulfate monotonically decreased with the reaction time and showed a redshift in the fluorescence band at Ex/Em = (250–300)/(400–500). Previous studies uncovered that the emission wavelengths of 400–500 nm are the indicative of humic-like substances (HULIS), which can significantly contribute to the light-absorbing properties of organic aerosols (Bianco et al., 2014). Previous studies revealed that the oxidation of non-photolyzable phenolics by  $\bullet\text{OH}$  can yield HULIS-like fluorescent products (Tang et al., 2020; Chang et al., 2010). Here, multi-hydroxy products from p-tolyl sulfate (e.g.,  $\text{C}_7\text{H}_7\text{O}_5\text{S}^-$ ,  $\text{C}_7\text{H}_7\text{O}_6\text{S}^-$

295

300

305

and  $C_7H_7O_7S^-$ ) and 4-ethylphenyl sulfate (e.g.,  $C_8H_9O_5S^-$ ,  $C_8H_9O_6S^-$  and  $C_8H_9O_7S^-$ ) may exhibit spectral features resembling aerosol HULIS.

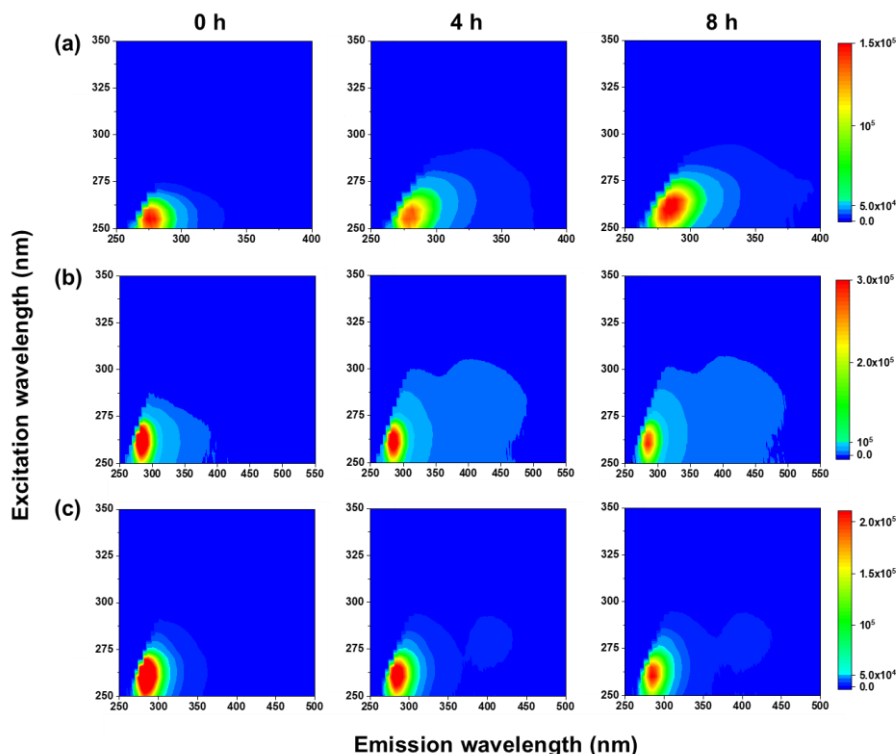


**Figure 4. Time profile of excitation–emission matrix (EEM) fluorescence spectra during the processes of (a) phenyl sulfate, (b) p-tolyl sulfate and (c) 4-ethylphenyl sulfate reacting with  $\bullet OH$  at pH 3.**

Employing phenyl sulfate as the representative, spectral changes at pH 8 were also examined. Previous studies have demonstrated that the light absorption properties of carbonyl compounds (e.g., aldehydes) and nitrophenols exhibit pronounced pH-dependence owing to protonation-deprotonation equilibria (Calvert and Schnitzler, 2023; Chen et al., 2020b). In this study, the phenyl sulfate remains deprotonated across the pH range of 3–8, resulting in negligible spectral variations in the initial solution (Figs. S9 and S13). However, the temporal evolution of the reaction revealed substantially enhanced absorbance at pH 3 compared to pH 8, particularly within the 300–400 nm range. Figure S14 shows the molecular composition of chromophores from the reaction of phenyl sulfate with  $\bullet OH$  at pH 8. Chromophores #1–3 were identical to those at pH 3 but exhibited stronger absorption due to their higher concentrations. An additional chromophore #4, eluting at 4.99–5.23 min, contributed significantly to absorption but the detailed composition of this chromophore is unknown. Compared to pH 3, solution of pH 8 exhibited an enhanced peak intensity at 4.99–5.23 min, while the peak at 14.98–15.67 min was reduced, which corresponded to distinct changes in the relative contributions to total absorption. For fluorescence spectra, phenyl sulfate exhibited an initial maximum fluorescence peak at  $Ex/Em = 255/279$  nm at pH 8 (Fig. S15), displaying minimal variation from the pH 3 conditions (Fig. 4a). However, the temporal evolution of its fluorescence spectrum differs obviously at different pH

values. Under basic conditions (pH 8), fluorescence decreased monotonically without recovery, and no red shift occurred even  
325 after 8 h.

#### 4 Atmospheric implications and conclusions

The current study investigated the liquid-phase reactions of three aromatic OSs (i.e., phenyl sulfate, p-tolyl sulfate, and 4-ethylphenyl sulfate) with •OH. It is found that functionalized and fragmented OSs as well as inorganic sulfate can be yielded during the reactions. The formation of functionalized OSs can enhance light absorption, thereby influencing aerosol optical  
330 properties. Fragmented OS formation resulting from ring-opening pathways during •OH oxidation of aromatic OSs has not reported previously. Several fragmented OSs (e.g.,  $C_2H_3O_5S^-$ ,  $C_5H_7O_8S^-$ ,  $C_4H_5O_7S^-$ , and  $C_5H_5O_6S^-$ ) detected in our study have been previously identified in ambient aerosols (Kuang et al., 2016; Cai et al., 2020; Wang et al., 2022; Yang et al., 2023), suggesting that aromatic OSs may serve as a potential source for aliphatic OSs in the atmosphere. Furthermore, the observation of inorganic sulfate formation, for the first time, indicates that aromatic OSs can also be converted into inorganic sulfate in  
335 analogy to aliphatic OSs (Kwong et al., 2018; Xu et al., 2022, 2024; Lai et al., 2025), potentially contributing to the atmospheric sulfur cycle. Further investigations are warranted to examine whether the proposed mechanism can be also applied to other types of aromatic OSs in the atmosphere.

The results of kinetic measurements reveal that aromatic OSs can react rapidly with •OH. As shown in Table S5, using the  $k$  values coupled with modeled •OH concentrations (Herrmann et al., 2005, 2010), the corresponding lifetimes ( $\tau=1/k_{OS}\times[•OH]$ )  
340 of aromatic OSs can be calculated. In urban areas, the concentrations of •OH in cloud and aerosol are estimated as  $3.5 \times 10^{-15}$  and  $4.4 \times 10^{-13}$  M, respectively. In contrast to urban areas, remote areas exhibit higher •OH concentrations both in cloud ( $2.2 \times 10^{-14}$  M) and aerosol ( $3.0 \times 10^{-12}$  M) (Herrmann et al., 2005, 2010). Concentrations of •OH are consistently higher in aerosol than in cloud water across different environments. Consequently, the lifetimes of aromatic OSs range from approximately 1 min in remote aerosols to up to 16 h in urban cloud water (Table S5), highlighting the significant influence  
345 of environmental conditions on their persistence. Previous studies reported that the lifetimes of aliphatic OSs in such varied environments range from several minutes to dozen days (Gweme and Styler, 2024; Lai et al., 2025). The substantially shorter lifetimes of aromatic OSs can be attributed to their higher reactivity toward OH radicals compared to aliphatic OSs. Given the high abundance of aromatic OSs and their fast reactivity with •OH in urban environments, aromatic OSs likely play a significant role in both the atmospheric sulfur cycle and environmental effects. In addition to lifetimes in aqueous environments,  
350 previous studies also estimated the atmospheric lifetimes of several aliphatic OSs via heterogeneous •OH oxidation based on measured uptake coefficients (Kwong et al., 2018; Lam et al., 2019; Xu et al., 2022). For instance, the atmospheric lifetime of methyl sulfate ranges from 53 min to 32 days via liquid-phase OH radical oxidation, compared to approximately 20 days via heterogeneous •OH oxidation (Gweme and Styler, 2024; Kwong et al., 2018). The results indicate that the atmospheric lifetimes of these OSs differ between liquid-phase and heterogeneous •OH oxidation pathways. However, experiments of

355 heterogeneous reactions of aromatic OSs with •OH were not conducted in this study. Thus, we cannot directly compare the lifetime of aromatic and aliphatic OSs through heterogeneous •OH oxidation, and need further investigations.

*Data availability.* Data are available upon request from the corresponding author.

*Supplement.* The supplement related to this article is available online.

*Author contributions.* LH designed research. YY, CY RY, PL, HZ, and HC, performed research. YY and LH analyzed data.  
360 YY and LH wrote the paper. LX, CY, YW, YZ, and HS provided valuable comments and suggestions for the manuscript.

*Competing interests.* The contact author has declared that none of the authors has any competing interests.

*Acknowledgements.* This study was financially supported by the National Key Research and Development Program of China (2022YFC3701102), the National Natural Science Foundation of China (42207121), the Outstanding Young Scholar of the Natural Science Foundation of Shandong Province, China (Overseas) (2022HWYQ-010), the Natural Science Foundation of  
365 Shandong Province (ZR2024YQ046). Liubin Huang gratefully acknowledges the support of the Program for Taishan Young Scholar (tsqz20221107).

## References

- Arciva, S., Niedek, C., Mavis, C., Yoon, M., Sanchez, M. E., Zhang, Q., and Anastasio, C.: Aqueous •OH oxidation of highly substituted phenols as a source of secondary organic aerosol, *Environ. Sci. Technol.*, 56, 9959–9967,  
370 <https://doi.org/10.1021/acs.est.2c02225>, 2022.
- Arciva, S., Ma, L., Mavis, C., Guzman, C., and Anastasio, C.: Formation and loss of light absorbance by phenolic aqueous SOA by •OH and an organic triplet excited state, *Atmos. Chem. Phys.*, 24, 4473–4485, <https://doi.org/10.5194/acp-24-4473-2024>, 2024.
- Armstrong, N. C.; Chen, Y.; Cui, T.; Zhang, Y.; Christensen, C.; Zhang, Z.; Turpin, B. J.; Chan, M. N.; Gold, A.; Ault, A. P.  
375 Isoprene epoxydiol-derived sulfated and nonsulfated oligomers suppress particulate mass loss during oxidative aging of secondary organic aerosol. *Environ. Sci. Technol.* 2022, 56, 16611.
- Baltaretu, C. O., Lichtman, E. I., Hadler, A. B., and Elrod, M. J.: Primary atmospheric oxidation mechanism for toluene, *J. Phys. Chem. A*, 113, 221–230, <https://doi.org/10.1021/jp806841t>, 2009.
- Bianco, A., Minella, M., Laurentiis, E. D., Maurino, V., Minero, C., and Vione, D.: Photochemical generation of photoactive  
380 compounds with fulvic-like and humic-like fluorescence in aqueous solution, *Chemosphere*, 111, 529–536, <https://doi.org/10.1016/j.chemosphere.2014.04.035>, 2014.
- Bloss, C., Wagner, V., Jenkin, M. E., Volkamer, R., Bloss, W. J., Lee, J. D., Heard, D. E., Wirtz, K., Martin-Reviejo, M., Rea, G., Wenger, J. C., and Pilling, M. J.: Development of a detailed chemical mechanism (MCMv3.1) for the atmospheric oxidation of aromatic hydrocarbons, *Atmos. Chem. Phys.*, 5, 641–664, <https://doi.org/10.5194/acp-5-641-2005>, 2005.

- 385 Buxton, G. V., Greenstock, C. L., Helman, W. P., and Ross, A. B.: Critical review of rate constants for reactions of hydrated electrons, hydrogen atoms and hydroxyl radicals ( $\bullet\text{OH}/\bullet\text{O}^-$  in aqueous solution, *J. Phys. Chem. Ref. Data*, 17, 513–886, <https://doi.org/10.1063/1.555805>, 1988.
- Cai, D., Wang, X., Chen, J., and Li, X.: Molecular characterization of organosulfates in highly polluted atmosphere using ultra-high-resolution mass spectrometry, *J. GEOPHYS. RES.-ATMOS.*, 125, e2019JD032253, <https://doi.org/10.1029/2019JD032253>, 2020.
- 390 Calvert, C. T., and Schnitzler, E. G.: Light absorption by cinnamaldehyde constituents of biomass burning organic aerosol modeled using time-dependent density functional theory, *ACS Earth Space Chem.*, 7, 490–500, <https://doi.org/10.1021/acsearthspacechem.2c00344>, 2023.
- Cao, T., Li, M., Xu, C., Song, J., Fan, X., Li, J., Jia, W., and Peng, P.: Technical note: Chemical composition and source identification of fluorescent components in atmospheric water-soluble brown carbon by excitation–emission matrix spectroscopy with parallel factor analysis – potential limitations and applications, *Atmos. Chem. Phys.*, 23, 2613–2625, <https://doi.org/10.5194/acp-23-2613-2023>, 2023.
- 395 Chang, J. L., and Thompson, J. E.: Characterization of colored products formed during irradiation of aqueous solutions containing  $\text{H}_2\text{O}_2$  and phenolic compounds, *Atmos. Environ.*, 44, 541–551, <https://doi.org/10.1016/j.atmosenv.2009.10.042>, 2010.
- 400 Chen, Y., Zhang, Y., Lambe, A. L., Xu, R., Lei, Z., Olson, N. E., Zhang, Z., Szalkowski, T., Cui, T., Vizueté, W., Gold, A., Turpin, B. J., Ault, A. P., Chan, M. N., Surratt, J. D.: Heterogeneous hydroxyl radical oxidation of isoprene-epoxydiol-derived methyltetrol sulfates: Plausible formation mechanisms of previously unexplained organosulfates in ambient fine aerosols, *Environ. Sci. Technol. Lett.*, 7, 460–468, <https://doi.org/10.1021/acs.estlett.0c00276>, 2020a.
- 405 Chen, J. Y., Rodriguez, E., Jiang, H., Chen, K., Frie, A., Zhang, H., Bahreini, R., and Lin, Y-H.: Time-dependent density functional theory investigation of the UV–Vis spectra of organonitrogen chromophores in brown carbon, *ACS Earth Space Chem.*, 4, 311–320, <https://doi.org/10.1021/acsearthspacechem.9b00328>, 2020b.
- Darer, A. I., Cole-Filipiak, N. C., O'Connor, A. E., and Elrod, M. J.: Formation and stability of atmospherically relevant isoprene-derived organosulfates and organonitrates, *Environ. Sci. Technol.*, 45, 1895–1902, <https://doi.org/10.1021/es103797z>, 2011.
- 410 Dong, P., Chen, Z., Qin, X., and Gong, Y.: Water significantly changes the ring-cleavage process during aqueous photooxidation of toluene, *Environ. Sci. Technol.*, 55, 16316–16325, <https://doi.org/10.1021/acs.est.1c04770>, 2021.
- Dorfman, L. M., and Adams, G. E.: Reactivity of the hydroxyl radical in aqueous solutions, *National Bureau of Standards*, 76, 1973.
- 415 Forstner, H. J. L., Flagan, R. C., and Seinfeld, J. H.: Secondary organic aerosol from the photooxidation of aromatic hydrocarbons: Molecular composition, *Environ. Sci. Technol.*, 31, 1345–1358, <https://doi.org/10.1021/es9605376>, 1997.
- Garmash, O., Rissanen, M. P., Pullinen, I., Schmitt, S., Kausiala, O., Tillmann, R., Zhao, D., Percival, C., Bannan, T. J., Priestley, M., Hallquist, Å. M., Kleist, E., Kiendler-Scharr, A., Hallquist, M., Berndt, T., McFiggans, G., Wildt, J., Mentel,

- T. F., and Ehn, M.: Multi-generation OH oxidation as a source for highly oxygenated organic molecules from aromatics, *Atmos. Chem. Phys.*, 20, 515–537, <https://doi.org/10.5194/acp-20-515-2020>, 2020.
- 420 Gweme, D. T., and Styler, S. A.: OH radical oxidation of organosulfates in the atmospheric aqueous phase, *J. Phys. Chem. A*, 128, 9462–9475, <https://doi.org/10.1021/acs.jpca.4c02877>, 2024.
- Hansen, A. M. K., Kristensen, K., Nguyen, Q. T., Zare, A., Cozzi, F., Nøjgaard, J. K., Skov, H., Brandt, J., Christensen, J. H., Ström, J., Tunved, P., Krejci, R., and Glasius, M.: Organosulfates and organic acids in Arctic aerosols: speciation, annual variation and concentration levels, *Atmos. Chem. Phys.*, 14, 7807–7823, <https://doi.org/10.5194/acp-14-7807-2014>, 2014.
- 425 Harrison, A. W., Waterson, A. M., and De Bruyn, W. J.: Spectroscopic and photochemical properties of secondary brown carbon from aqueous reactions of methylglyoxal, *ACS Earth Space Chem.*, 4, 762–773, <https://doi.org/10.1021/acsearthspacechem.0c00061>, 2020.
- He, J., Li, L., Li, Y., Huang, M., Zhu, Y., and Deng, S.: Synthesis, MS/MS characteristics and quantification of six aromatic organosulfates in atmospheric PM<sub>2.5</sub>, *Atmos. Environ.*, 290, 119361, <https://doi.org/10.1016/j.atmosenv.2022.119361>, 2022.
- 430 Heath, A. A., Ehrenhauser, F. S., and Valsaraj, K. T.: Effects of temperature, oxygen level, ionic strength, and pH on the reaction of benzene with hydroxyl radicals in aqueous atmospheric systems, *Environ. Chem. Eng.*, 1, 822–830, <https://doi.org/10.1016/j.jece.2013.07.023>, 2013.
- 435 Hems, R. F., and Abbatt, J. P. D.: Aqueous phase photo-oxidation of brown carbon nitrophenols: Reaction kinetics, mechanism, and evolution of light absorption, *ACS Earth Space Chem.*, 2, 225–234, <https://doi.org/10.1021/acsearthspacechem.7b00123>, 2018.
- Herrmann, H., Schaefer, T., Tilgner, A., Styler, S. A., Weller, C., Teich, M., and Otto, T.: Tropospheric aqueous-phase chemistry: kinetics, mechanisms, and its coupling to a changing gas phase, *Chem. Rev.*, 115, 4259–4334, <https://doi.org/10.1021/cr500447k>, 2015.
- 440 Herrmann, H., Tilgner, A., Barzaghi, P., Majdik, Z., Gligorovski, S., Poulain, L., and Monod, A.: Towards a more detailed description of tropospheric aqueous phase organic chemistry: CAPRAM 3.0, *Atmos. Environ.*, 39, 4351–4363, <https://doi.org/10.1016/j.atmosenv.2005.02.016>, 2005.
- Herrmann, H., Hoffmann, D., Schaefer, T., Bräuer, P., and Tilgner, A.: Tropospheric aqueous-phase free-radical chemistry: Radical sources, spectra, reaction kinetics and prediction tools, *ChemPhysChem*, 11, 3796–3822, <https://doi.org/10.1002/cphc.201000533>, 2010.
- 445 Hettiyadura, A. P. S., Al-Naiema, I. M., Hughes, D. D., Fang, T., and Stone, E. A.: Organosulfates in Atlanta, Georgia: anthropogenic influences on biogenic secondary organic aerosol formation, *Atmos. Chem. Phys.*, 19, 3191–3206, <https://doi.org/10.5194/acp-19-3191-2019>, 2019.
- 450 Hettiyadura, A. P. S., Jayarathne, T., Baumann, K., Goldstein, A. H., de Gouw, J. A., Koss, A., Keutsch, F. N., Skog, K., and Stone, E. A.: Qualitative and quantitative analysis of atmospheric organosulfates in Centreville, Alabama, *Atmos. Chem. Phys.*, 17, 1343–1359, <https://doi.org/10.5194/acp-17-1343-2017>, 2017.

- Hu, K. S., Darer, A. I., and Elrod, M. J.: Thermodynamics and kinetics of the hydrolysis of atmospherically relevant organonitrates and organosulfates, *Atmos. Chem. Phys.*, 11, 8307–8320, <https://doi.org/10.5194/acp-11-8307-2011>, 2011.
- 455 Hu, W. W., Campuzano-Jost, P., Palm, B. B., Day, D. A., Ortega, A. M., Hayes, P. L., Krechmer, J. E., Chen, Q., Kuwata, M., Liu, Y. J., de Sá, S. S., McKinney, K., Martin, S. T., Hu, M., Budisulistiorini, S. H., Riva, M., Surratt, J. D., St. Clair, J. M., Isaacman-Van Wertz, G., Yee, L. D., Goldstein, A. H., Carbone, S., Brito, J., Artaxo, P., de Gouw, J. A., Koss, A., Wisthaler, A., Mikoviny, T., Karl, T., Kaser, L., Jud, W., Hansel, A., Docherty, K. S., Alexander, M. L., Robinson, N. H., Coe, H., Allan, J. D., Canagaratna, M. R., Paulot, F., and Jimenez, J. L.: Characterization of a real-time tracer for isoprene epoxydiols-derived secondary organic aerosol (IEPOX-SOA) from aerosol mass spectrometer measurements, *Atmos. Chem. Phys.*, 15, 11807–11833, <https://doi.org/10.5194/acp-15-11807-2015>, 2015.
- 460 Huang, L., Cochran, R. E., Coddens, E. M., and Grassian, V. H.: Formation of organosulfur compounds through transition metal ion-catalyzed aqueous phase reactions, *Environ. Sci. Technol. Lett.*, 5, 315–321, <https://doi.org/10.1021/acs.estlett.8b00225>, 2018.
- 465 Huang, L., Wang, Y., Zhao, Y., Hu, H., Yang, Y., Wang, Y., Yu, J.-Z., Chen, T., Cheng, Z., Li, C., and Xiao, H.: Biogenic and anthropogenic contributions to atmospheric organosulfates in a typical megacity in eastern China, *J GEOPHYS RES-ATMOS*, 128, e2023JD038848, <https://doi.org/10.1029/2023JD038848>, 2023.
- Iinuma, Y., Müller, C., Berndt, T., Böge, O., Claeys, M., and Herrmann, H.: Evidence for the existence of organosulfates from  $\beta$ -Pinene ozonolysis in ambient secondary organic aerosol, *Environ. Sci. Technol.*, 41, 6678–6683, <https://doi.org/10.1021/es070938t>, 2007.
- 470 Kuang, B. Y., Lin, P., Hu, M., and Yu, J., Z.: Aerosol size distribution characteristics of organosulfates in the Pearl River Delta region, China, *Atmos. Environ.*, 130, 23–35, <https://doi.org/10.1016/j.atmosenv.2015.09.024>, 2016.
- Kundu, S., Quraishi, T. A., Yu, G., Suarez, C., Keutsch, F. N., and Stone, E. A.: Evidence and quantitation of aromatic organosulfates in ambient aerosols in Lahore, Pakistan, *Atmos. Chem. Phys.*, 13, 4865–4875, <https://doi.org/10.5194/acp-13-4865-2013>, 2013.
- 475 Kwong, K. C., Chim, M. M., Davies, J. F., Wilson, K. R., and Chan, M. N.: Importance of sulfate radical anion formation and chemistry in heterogeneous  $\bullet$ OH oxidation of sodium methyl sulfate, the smallest organosulfate, *Atmos. Chem. Phys.*, 18, 2809–2820, <https://doi.org/10.5194/acp-18-2809-2018>, 2018.
- Kristensen, K., and Glasius, M.: Organosulfates and oxidation products from biogenic hydrocarbons in fine aerosols from a forest in north west Europe during spring, *Atmos. Environ.*, 45, 4546–4556, <https://doi.org/10.1016/j.atmosenv.2011.05.063>, 2011.
- Lai, D., Schaefer, T., Zhang, Y., Li, Y. J., Xing, S., Herrmann, H., and Chan, M. N.: Deactivating effect of hydroxyl radicals reactivity by sulfate and sulfite functional groups in aqueous phase—atmospheric implications for small organosulfur compounds, *ACS EST Air*, 1, 678–689, <https://doi.org/10.1021/acsestair.4c00033>, 2024.
- 485 Lai, D., Bai, Y., Zhang, Z., So, P.-K., Li, Y. J., Tse, Y.-L. S., Yeung, Y.-Y., Schaefer, T., Herrmann, H., Yu, J. Z., Wang, Y., and Chan, M. N.: Rapid aqueous-phase oxidation of an  $\alpha$ -pinene-derived organosulfate by hydroxyl radicals: a potential

- source of some unclassified oxygenated and small organosulfates in the atmosphere, *Atmos. Chem. Phys.*, 25, 12569–12584, <https://doi.org/10.5194/acp-25-12569-2025>, 2025.
- 490 Laskin, A., Laskin, J., and Nizkorodov, S. A.: Chemistry of atmospheric brown carbon, *Chem. Rev.*, 115, 4335–4382, <https://doi.org/10.1021/cr5006167>, 2015.
- Lay, T. H., Bozzelli, J. W., and Seinfeld, J. H.: Atmospheric photochemical oxidation of benzene: benzene + OH and the benzene–OH adduct (hydroxyl-2,4-cyclohexadienyl) + O<sub>2</sub>, *J. Phys. Chem.*, 100, 6543–6554, <https://doi.org/10.1021/jp951726y>, 1996.
- 495 Lei, Z., Chen, Y., Zhang, Y., Cooke, M. E., Ledsky, I. R., Armstrong, N. C., Olson, N. E., Zhang, Z., Gold, A., Surratt, J. D., and Ault, A. P.: Initial pH governs secondary organic aerosol phase state and morphology after uptake of isoprene epoxydiols (IEPOX), *Environ. Sci. Technol.*, 56, 10596–10607, <https://doi.org/10.1021/acs.est.2c01579>, 2022.
- Li, F., Tsona, N. T., Li, J., and Du, L.: Aqueous-phase oxidation of syringic acid emitted from biomass burning: Formation of light-absorbing compounds, *Sci. Total Environ.*, 765, 144239, <https://doi.org/10.1016/j.scitotenv.2020.144239>, 2021.
- 500 Li, S., Wang, Y., Zhang, Y., Yi, Y., Wang, Y., Guo, Y., Yu, C., Jiang, Y., Shi, J., Zhang, C., Zhu, J., Hu, W., Yu, J., Yao, X., Gao, H., and Hu, M.: Atmospheric organosulfate formation regulated by continental outflows and marine emissions over East Asian marginal seas, *Atmos. Chem. Phys.*, 25, 12585–12598, <https://doi.org/10.5194/acp-25-12585-2025>, 2025.
- Liu, F., Xu, T., Ng, N. L., and Lu, H.: Linking cell health and reactive oxygen species from secondary organic aerosols exposure, *Environ. Sci. Technol.*, 57, 1039–1048, <https://doi.org/10.1021/acs.est.2c05171>, 2022.
- 505 Liu, G., Ji, J., Huang, H., Xie, R., Feng, Q., Shu, Y., Zhan, Y., Fang, R., He, M., Liu, S., Ye, X., and Leung, D. Y. C.: UV/H<sub>2</sub>O<sub>2</sub>: An efficient aqueous advanced oxidation process for VOCs removal, *Chem. Eng. J.*, 324, 44–50, <https://doi.org/10.1016/j.cej.2017.04.105>, 2017.
- Lin, Y.-H., Knipping, E. M., Edgerton, E. S., Shaw, S. L., and Surratt, J. D.: Investigating the influences of SO<sub>2</sub> and NH<sub>3</sub> levels on isoprene-derived secondary organic aerosol formation using conditional sampling approaches, *Atmos. Chem. Phys.*, 13, 8457–8470, <https://doi.org/10.5194/acp-13-8457-2013>, 2013.
- 510 Lukács, H., Gelencsér, A., Hoffer, A., Kiss, G., Horváth, K., and Hartyáni, Z.: Quantitative assessment of organosulfates in size-segregated rural fine aerosol, *Atmos. Chem. Phys.*, 9, 231–238, <https://doi.org/10.5194/acp-9-231-2009>, 2009.
- Ma, J., Reininger, N., Zhao, C., Döbler, D., Rüdiger, J., Qiu, Y., Ungeheuer, F., Simon, M., D’Angelo, L., Breuninger, A., David, J., Bai, Y., Li, Y., Xue, Y., Li, L., Wang, Y., Hildmann, S., Hoffmann, T., Liu, B., Niu, H., Wu, Z., and Vogel, A. L.: Unveiling a large fraction of hidden organosulfates in ambient organic aerosol, *Nat. Commun.*, 16, 4098, <https://doi.org/10.1038/s41467-025-59420-y>, 2025.
- 515 Ma, Y., Xu, X., Song, W., Geng, F., and Wang, L.: Seasonal and diurnal variations of particulate organosulfates in urban Shanghai, China, *Atmos. Environ.*, 85, 152–160, <https://doi.org/10.1016/j.atmosenv.2013.12.017>, 2014.
- Mael, L. E., Jacobs, M. I., and Elrod, M. J.: Organosulfate and nitrate formation and reactivity from epoxides derived from 2-Methyl-3-buten-2-ol, *J. Phys. Chem. A*, 119, 4464–4472, <https://doi.org/10.1021/jp510033s>, 2015.
- 520 Minakata, D., Song, W., Mezyk, S. P., and Cooper, W. J.: Experimental and theoretical studies on aqueous-phase reactivity of

- hydroxyl radicals with multiple carboxylated and hydroxylated benzene compounds, *Phys. Chem. Chem. Phys.*, 17, 11796–11812, <https://doi.org/10.1039/C5CP00861A>, 2015.
- Minerath, E. C., Casale, M. T., and Elrod, M. J.: Kinetics feasibility study of alcohol sulfate esterification reactions in tropospheric aerosols, *Environ. Sci. Technol.*, 42, 4410–4415, <https://doi.org/10.1021/es8004333>, 2008.
- 525 Monod, A., and Doussin, J. F.: Structure-activity relationship for the estimation of OH-oxidation rate constants of aliphatic organic compounds in the aqueous phase: alkanes, alcohols, organic acids and bases, *Atmos. Environ.*, 42, 7611–7622, <https://doi.org/10.1016/j.atmosenv.2008.06.005>, 2008.
- Nozière, B., Ekström, S., Alsberg, T., and Holmström S.: Radical-initiated formation of organosulfates and surfactants in atmospheric aerosols, *Geophys. Res. Lett.*, 37, L05806, <https://doi.org/10.1029/2009GL041683>, 2010.
- 530 Pan, X-M., Schuchmann, M. N., and Sonntag, C. V.: Oxidation of benzene by the OH radical. A product and pulse radiolysis study in oxygenated aqueous solution, *J. Chem. Soc., Perkin Trans.*, 2, 289–297, <https://doi.org/10.1039/P29930000289>, 1993.
- Passananti, M., Kong, L., Shang, J., Dupart, Y., Perrier, S., Chen, J., Donaldson, J., and George, C.: Organosulfate formation through the heterogeneous reaction of sulfur dioxide with unsaturated fatty acids and long-chain alkenes, *Angew. Chem. Int. Ed.*, 55, 10336–10339, <https://doi.org/10.1002/anie.201605266>, 2016.
- 535 Peng, X., Xie, T-T., Tang, M-X., Cheng, Y., Peng, Y., Wei, F-H., Cao, L-M., Yu, K., Du, K., He, L-Y., and Huang, X-F.: Critical role of secondary organic aerosol in urban atmospheric visibility improvement identified by machine learning, *Environ. Sci. Technol. Lett.*, 10, 976–982, <https://doi.org/10.1021/acs.estlett.3c00084>, 2023.
- Pye, H. O. T., Nenes, A., Alexander, B., Ault, A. P., Barth, M. C., Clegg, S. L., Collett Jr., J. L., Fahey, K. M., Hennigan, C. J., Herrmann, H., Kanakidou, M., Kelly, J. T., Ku, I.-T., McNeill, V. F., Riemer, N., Schaefer, T., Shi, G., Tilgner, A., Walker, J. T., Wang, T., Weber, R., Xing, J., Zaveri, R. A., and Zuend, A.: The acidity of atmospheric particles and clouds, *Atmos. Chem. Phys.*, 20, 4809–4888, <https://doi.org/10.5194/acp-20-4809-2020>, 2020.
- 540 Riva, M., Chen, Y., Zhang, Y., Lei, Z., Olson, N. E., Boyer, H. C., Narayan, S., Yee, L. D., Green, H. S., Cui, T., Zhang, Z., Baumann, K., Fort, M., Edgerton, E., Budisulistiorini, S. H., Rose, C. A., Ribeiro, I. O., e Oliveira, R. L., dos Santos, E. O., Machado, C. M. D., Szopa, S., Zhao, Y., Alves, E. G., de Sá, S. S., Hu, W., Knipping, E. M., Shaw, S. L., Junior, S. D., de Souza, R. A. F., Palm, B. B., Jimenez, J-L., Glasius, M., Goldstein, A. H., Pye, H. O. T., Gold, A., Turpin, B. J., Vizuete, W., Martin, S. T., Thornton, J. A., Dutcher, C. S., Ault, A. P., and Surratt, J. D.: Increasing isoprene epoxydiol-to-inorganic sulfate aerosol ratio results in extensive conversion of inorganic sulfate to organosulfur forms: Implications for aerosol physicochemical properties, *Environ. Sci. Technol.*, 53, 8682–8694, <https://doi.org/10.1021/acs.est.9b01019>,
- 550 2019.
- Schindelka, J., Iinuma, Y., Hoffmann, D., and Herrmann, H.: Sulfate radical-initiated formation of isoprene-derived organosulfates in atmospheric aerosols, *Faraday Discuss.*, 165, 237–259, <https://doi.org/10.1039/C3FD00042G>, 2013.
- Schuler, R. H., and Albarran, G.: The rate constants for reaction of radical •OH radicals with benzene and toluene, *Radiat. Phys. Chem.*, 64, 189–195, [https://doi.org/10.1016/S0969-806X\(01\)00497-2](https://doi.org/10.1016/S0969-806X(01)00497-2), 2002.

- 555 Shang, J., Passananti, M., Dupart, Y., Ciuraru, R., Tinel, L., Rossignol, S., Perrier, S., Zhu, T., and George, C.: SO<sub>2</sub> uptake on oleic acid: A new formation pathway of organosulfur compounds in the atmosphere, *Environ. Sci. Technol. Lett.*, 3, 67–72, <https://doi.org/10.1021/acs.estlett.6b00006>, 2016.
- Shrivastava, M., Cappa, C. D., Fan, J., Goldstein, A. H., Guenther, A. B., Jimenez, J. L., Kuang, C., Laskin, A., Martin, S. T., Ng, N. L., Petaja, T., Pierce, J. R., Rasch, P. J., Roldin, P., Seinfeld, J. H., Shilling, J., Smith, J. N., Thornton, J. A., Volkamer, R., Wang, J., Worsnop, D. R., Zaveri, R. A., Zelenyuk, A., and Zhang, Q.: Recent advances in understanding secondary organic aerosol: Implications for global climate forcing, *Rev. Geophys.*, 55, 509–559, <https://doi.org/10.1002/2016RG000540>, 2017.
- 560 Singla, R., Ashokkumar, M., and Grieser, F.: The mechanism of the sonochemical degradation of benzoic acid in aqueous solutions, *Res. Chem. Intermed.*, 30, 723–733, <https://doi.org/10.1163/1568567041856963>, 2004.
- 565 Smith, J. D., Kinney, H., and Anastasio, C.: Aqueous benzene-diols react with an organic triplet excited state and hydroxyl radical to form secondary organic aerosol, *Phys. Chem. Chem. Phys.*, 17, 10227–10237, <https://doi.org/10.1039/C4CP06095D>, 2015.
- Surratt, J. D., Gómez-González, Y., Chan, A. W. H., Vermeylen, R., Shahgholi, M., Kleindienst, T. E., Edney, E. O., Offenberg, J. H., Lewandowski, M., Jaoui, M., Maenhaut, W., Claeys, M., Flagan, R. C., and Seinfeld, J. H.: Organosulfate formation in biogenic secondary organic aerosol, *J. Phys. Chem. A*, 112, 8345–8378, <https://doi.org/10.1021/jp802310p>, 2008.
- 570 Surratt, J. D., Chan, A. W. H., Eddingsaas, N.C., and Seinfeld, J. H.: Reactive intermediates revealed in secondary organic aerosol formation from isoprene, *Proc. Natl. Acad. Sci. U.S.A.*, 107, 6640–6645, <https://doi.org/10.1073/pnas.0911114107>, 2010.
- Tang, S., Li, F., Tsona, N. T., Lu, C. Y., Wang, X. F., and Du, L.: Aqueous-phase photooxidation of vanillic acid: A potential source of Humic-Like Substances (HULIS), *ACS Earth Space Chem.*, 4, 862–872, <https://doi.org/10.1021/acsearthspacechem.0c00070>, 2020.
- Thomas, A. E., Glicker, H. S., Guenther, A. B., Seco, R., Vega Bustillos, O., Tota, J., Souza, R. A. F., and Smith, J. N.: Seasonal investigation of ultrafine-particle organic composition in an eastern Amazonian rainforest, *Atmos. Chem. Phys.*, 25, 959–977, <https://doi.org/10.5194/acp-25-959-2025>, 2025.
- 580 Tolocka, M. P., and Turpin, B.: Contribution of organosulfur compounds to organic aerosol mass, *Environ. Sci. Technol.*, 46, 7978–7983, <https://doi.org/10.1021/es300651v>, 2012.
- Tsona T. N., Lv, X., Tasheh, S. N., Ghogomu, J. N., and Du, L.: Atmospheric fate of organosulfates through gas-phase and aqueous-phase reactions with hydroxyl radicals: implications for inorganic sulfate formation, *Atmos. Chem. Phys.*, 25, 8575–8590, <https://doi.org/10.5194/acp-25-8575-2025>, 2025.
- 585 Wang, L., Wu, R., and Xu, C.: Atmospheric oxidation mechanism of benzene. fates of alkoxy radical intermediates and revised mechanism, *J. Phys. Chem. A*, 117, 14163–14168, <https://doi.org/10.1021/jp4101762>, 2013.
- Wang, S., Zhou, S., Tao, Y., Tsui, W. G., Ye, J., Yu, J.Z., Murphy, J. G., McNeill, V. F., Abbatt, J. P. D., and Chan, A. W. H.: Organic peroxides and sulfur dioxide in aerosol: source of particulate sulfate, *Environ. Sci. Technol.*, 53, 10695–10704,

<https://doi.org/10.1021/acs.est.9b02591>, 2019.

- 590 Wang, Y., Hu, M., Guo, S., Wang, Y., Zheng, J., Yang, Y., Zhu, W., Tang, R., Li, X., Liu, Y., Le Breton, M., Du, Z., Shang, D.,  
Wu, Y., Wu, Z., Song, Y., Lou, S., Hallquist, M., and Yu, J.: The secondary formation of organosulfates under interactions  
between biogenic emissions and anthropogenic pollutants in summer in Beijing, *Atmos. Chem. Phys.*, 18, 10693–10713,  
<https://doi.org/10.5194/acp-18-10693-2018>, 2018. Wang, Y., Ma, Y., Kuang, B., Lin, P., Liang, Y., Huang, C., and Yu, J.  
Z.: Abundance of organosulfates derived from biogenic volatile organic compounds: Seasonal and spatial contrasts at four  
595 sites in China, *Sci. Total Environ.*, 806, 151275, <https://doi.org/10.1016/j.scitotenv.2021.151275>, 2022.
- Wang, Y., Zhao, Y., Wang, Y., Yu, J.-Z., Shao, J., Liu, P., Zhu, W., Cheng, Z., Li, Z., Yan, N., and Xiao, H.: Organosulfates in  
atmospheric aerosols in Shanghai, China: seasonal and interannual variability, origin, and formation mechanisms, *Atmos.  
Chem. Phys.*, 21, 2959–2980, <https://doi.org/10.5194/acp-21-2959-2021>, 2021.
- Xu, R., Ge, Y., Kwong, K. C., Poon, H. Y., Wilson, K. R., Yu, J. Z., and Chan, M. N.: Inorganic sulfur species formed upon  
600 heterogeneous •OH oxidation of organosulfates: A case study of methyl sulfate, *ACS Earth Space Chem.*, 4, 2041–2049,  
<https://doi.org/10.1021/acsearthspacechem.0c00209>, 2020.
- Xu, R., Ng, S. I. M., Chow, W. S., Wong, Y. K., Wang, Y., Lai, D., Yao, Z., So, P.-K., Yu, J. Z., and Chan, M. N.: Chemical  
transformation of  $\alpha$ -pinene-derived organosulfate via heterogeneous OH oxidation: implications for sources and  
environmental fates of atmospheric organosulfates, *Atmos. Chem. Phys.*, 22, 5685–5700, [https://doi.org/10.5194/acp-22-](https://doi.org/10.5194/acp-22-5685-2022)  
605 [5685-2022](https://doi.org/10.5194/acp-22-5685-2022), 2022.
- Xu, R., Chen, Y., Ng, S. I. M., Zhang, Z., Gold, A., Turpin, B. J., Ault, A. P., Surratt, J.D., and Chan, M. N.: Formation of  
inorganic sulfate and volatile nonsulfated products from heterogeneous hydroxyl radical oxidation of 2-methyltetrol  
sulfate aerosols: Mechanisms and atmospheric implications, *Environ. Sci. Technol. Lett.*, 11, 968–974,  
<https://doi.org/10.1021/acs.estlett.4c00451>, 2024.
- 610 Yan, J.; Zhang, Y.; Chen, Y.; Armstrong, N. C.; Buchenau, N. A.; Lei, Z.; Xiao, Y.; Zhang, Z.; Lambe, A. T.; Chan, M. N. Kinetics  
and products of heterogeneous hydroxyl radical oxidation of isoprene epoxydiol-derived secondary organic aerosol. *ACS  
Earth Space Chem.* 2023, 7, 1916.
- Yang, T., Xu, Y., Ye, Q., Ma, Y.-J., Wang, Y.-C., Yu, J.-Z., Duan, Y.-S., Li, C.-X., Xiao, H.-W., Li, Z.-Y., Zhao, Y., and Xiao,  
H.-Y.: Spatial and diurnal variations of aerosol organosulfates in summertime Shanghai, China: potential influence of  
615 photochemical processes and anthropogenic sulfate pollution, *Atmos. Chem. Phys.*, 23, 13433–13450,  
<https://doi.org/10.5194/acp-23-13433-2023>, 2023.
- Yao, M., Zhao, Y., Hu, M., Huang, D., Wang, Y., Yu, J. Z., and Yan, N.: Multiphase reactions between secondary organic  
aerosol and sulfur dioxide: kinetics and contributions to sulfate formation and aerosol aging, *Environ. Sci. Technol. Lett.*,  
6, 768–774, <https://doi.org/10.1021/acs.estlett.9b00657>, 2019.
- 620 Yao, M., Zhao, Y., Chang, C. X., Wang, S., Li, Z., Li, C., Chan, A. W. H., and Xiao, H.: Multiphase reactions between organic  
peroxides and sulfur dioxide in internally mixed inorganic and organic particles: key roles of particle phase separation  
and acidity, *Environ. Sci. Technol.*, 57, 15558–15570, <https://doi.org/10.1021/acs.est.3c04975>, 2023.

625 Zhang, H., Worton, D. R., Lewandowski, M., Ortega, J., Rubitschun, C. L., Park, J-H., Kristensen, K., Campuzano-Jost, P., Day, D. A., Jimenez, J. L., Jaoui, M., Offenberg, J. H., Kleindienst, T. E., Gilman, T. E., Gilman, J., Kuster, W. C., Gouw, J., Park, C., Schade, G. W., Frossard, A. A., Russell, L., Kaser, L., Jud, W., Hansel, A., Cappellin, L., Karl, T., Glasius, M., Guenther, A., Goldstein, A. H., Seinfeld, J. H., Gold, A., Kamens, R. M., and Surratt, J. D.: Organosulfates as tracers for secondary organic aerosol (SOA) formation from 2-Methyl-3-Buten-2-ol (MBO) in the atmosphere, *Environ. Sci. Technol.*, 46, 9437–9446, <https://doi.org/10.1021/es301648z>, 2012.